Front. Comput. Sci., 2023, 17(2): 172702
https://doi.org/10.1007/s11704-022-1205-7

RESEARCH ARTICLE

Underwater image enhancement by maximum-likelihood based adaptive color correction and robust scattering removal

Bo WANG (✉)[1], Zitong KANG[1], Pengwei DONG[1], Fan WANG[1], Peng MA[1], Jiajing BAI[1], Pengwei LIANG[1], Chongyi LI[2]

1 School of Physics and Electronic-Electrical Engineering, Ningxia University, Yinchuan 750021, China
2 School of Computer Science and Engineering, Nanyang Technological University, Singapore 639798, Singapore

Abstract Underwater images often exhibit severe color deviations and degraded visibility, which limits many practical applications in ocean engineering. Although extensive research has been conducted into underwater image enhancement, little of which demonstrates the significant robustness and generalization for diverse real-world underwater scenes. In this paper, we propose an adaptive color correction algorithm based on the maximum likelihood estimation of Gaussian parameters, which effectively removes color casts of a variety of underwater images. A novel algorithm using weighted combination of gradient maps in HSV color space and absolute difference of intensity for accurate background light estimation is proposed, which circumvents the influence of white or bright regions that challenges existing physical model-based methods. To enhance contrast of resultant images, a piece-wise affine transform is applied to the transmission map estimated via background light differential. Finally, with the estimated background light and transmission map, the scene radiance is recovered by addressing an inverse problem of image formation model. Extensive experiments reveal that our results are characterized by natural appearance and genuine color, and our method achieves competitive performance with the state-of-the-art methods in terms of objective evaluation metrics, which further validates the better robustness and higher generalization ability of our enhancement model.

Keywords underwater image enhancement, adaptive color correction, background light estimation

1 Introduction

Images captured in underwater environments usually suffer from degraded quality in terms of severe color distortion, poor visibility and contrast. This is because floating particles in water lead to selective lighting absorption and scattering when the light propagates between the scene and the camera. With the rapid development of aquatic robot inspection, ocean engineer, marine archaeology and ecological research, the degraded underwater images seriously restrict the performance of various computer vision algorithms used for observation and analysis [1,2].

As a significant and challenging research task, underwater image enhancement has attracted much attention within the past decade [3−12]. In order to improve the quality of underwater images, a great variety of approaches have been presented and can be divided into three groups: image formation model (IFM)-based, non-IFM-based, and deep learning-based methods. Some existing methods treated the problem as image dehazing based on an IFM, mainly including the background light and the transmission map estimation, then achieved the clear images by solving an inverse problem based on the estimated IFM parameters [13−15]. Non-IFM-based approaches are designed to modify pixel values to improve visual effects, such as color correction and stretch of dynamic pixels range [16−18]. Recently, deep learning techniques achieve significant advance from low-level to high-level computer vision problems, which motivates various underwater image enhancement methods based on deep learning, especially generative adversarial networks (GANs) to be proposed and pushed forward [19−21].

Even though previous underwater image enhancement methods have obtained a measure of success, most of which only provide limited analysis and discussion about the robustness and generalization. Since multifarious underwater images with different degraded issues depend on complicated underwater environments, it is necessary to verify the effectiveness on various kinds of real-world underwater image datasets instead of some specific images. Besides, the performance of current underwater image enhancement methods based on deep learning still lag behind the traditional ones in terms of some indicators due to insufficient training data and network models not designed for this task. In other words, the deep learning-based methods just provide limited generalization capability to the real-world underwater images [1].

In this paper, we first propose an adaptive color correction algorithm for diverse underwater scenes including multi-types of greenish and bluish tone, low and high backscatter, and turbid images with severe degradations. Then, we adopt

Received April 27, 2021; accepted October 15, 2021

E-mail: tjuwb@nxu.edu.cn

weighted combination of gradient maps in HSV color space and absolute difference of intensity of grayscale images to accurately estimate the background light. To the best of our knowledge, it is the first time to use a map of background light estimation for obtaining the latent parameter of IFM. Next, a piece-wise affine transform is employed to enhance the estimated transmission map, which effectively boost the sharpness and contrast of final enhanced images. Since both of these two latent parameters (i.e., background light and transmission map) deciding the scattering removal effects are estimated from a given image, we can finally obtain the scene radiance (i.e., a haze-free image) via addressing an inverse problem based on IFM.

The remainder of this paper is organized as follows. In section 2, we review different methods for underwater image enhancement. Then, we provide parameters estimation of Gaussian model for adaptive color correction and details of the proposed method for background light estimation and transmission map enhancement in Section 3. In Section 4, some experimental results and analysis are described. Finally, the conclusion is presented and the future work is given in Section 5.

2 Related work

The past decade has witnessed the rapid development of underwater image enhancement. There are three mainstream approaches for the enhancement of underwater images comprising IFM-based, non-IFM-based, and deep learning-based methods.

2.1 IFM-based methods

Inspired by conventional terrestrial image dehazing schemes, some researchers concentrated on specialized underwater image restoration problems based on IFM in recent years. Carlevaris-Bianco et al. [22] employed the difference among the maximum intensity of the red, green and blue channels to estimate the depth information of a scene that was used to remove haze in underwater images. Chiang et al. [23] exploited wavelength compensation to restore underwater images by dehazing, which could simultaneously achieve color correction and dehazing. Lu et al. [24] proposed a novel IFM compensating for attenuation discrepancy along the path of propagation and developed a color-lines-based background light estimator for turbid underwater images. Based on the minimum information loss and histogram distribution prior, Li et al. [25] presented a method to enhance underwater images and obtained high contrast results. Peng et al. [26] proposed an approach to estimate underwater scene depth based on image blurriness and light absorption, which is used to enhance underwater images. Berman et al. [27] utilized spectral profiles of various water bodies for color constancy and evaluated this method on a new underwater image dataset. Based on adaptive attenuation-curve prior depending on statistical distribution of pixel values, Wang et al. [28] proposed an effective method for single underwater image restoration. Peng et al. [29] generalized the dark channel prior (DCP) based on depth-dependent color change for diverse degraded image restoration including underwater scene with different color casts and lighting conditions. However, it is hard to effectively remove color distortion for a wide range of underwater images by these existing IFM-based methods. To solve this issue, we propose an effective method as independent pre-processing step for color correction, which is applicable to diverse underwater scenes.

2.2 Non-IFM-based methods

Another line of research is straightforward to improve image quality and generate an enhanced image without IFM. Ancuti et al. [30] introduced a novel fusion-based strategy deriving the inputs and weights only from the original underwater scene without multiple images. Fu et al. [31] proposed a retinex-based approach which consists of three steps: color correction, decomposing the reflectance and the illumination, and post-processing for fuzz and under-exposure. Zhang et al. [32] employed an extended multi-scale retinex-based method (LAB-MSR) to process the underwater images in CIELAB color space. A two-step method for underwater image enhancement was presented in [33], which contains an effective color correcting strategy and a novel optimal contrast improvement. Ancuti et al. [34,35] proposed an approach to fuse the advantages of color balance and multiscale fusion strategy for underwater image enhancement. Then, color channel compensation (3C) as a pre-processing method is further discussed and employed for various image enhancement solutions. Although this type of enhancement technique obtains better global color correction for underwater images, it tends to produce visually unpleasing results (i.e., over enhancement or over saturation). By contrast, we treat color correction problem as a global color redistribution using parameters estimation of Gaussian model built on each color channel, which is different from the above methods and is able to generate natural results with genuine color.

2.3 Deep learning-based methods

Recently, deep learning substantially improves the performance of various low-level computer vision tasks including underwater image dehazing. Li et al. [36] employed synthetic training data to train a two-stage deep network, called WaterGAN, for underwater image enhancement. Based on Cycle-GAN [37], a weakly supervised color transfer model (i.e., Water Cycle-GAN) was proposed for underwater image color correction [38], which relaxes the unavailability of paired real-world training data. Guo et al. [39] proposed a residual multi-scale dense block using dense connections and residual learning in generator for underwater image enhancement. Li et al. [40] proposed an end-to-end CNN model, called UWCNNs, which is trained by synthetic underwater image datasets generated by the revised underwater image formation model. Fu et al. [2] introduced a two-branch network to compensate the global color distortion and local reduced contrast, and then the compressed histogram equalization was used to avoid the over-enhancement problem. Nonetheless, most of the deep learning-based methods are facing the problems that they have to follow the IFM or simplified underwater IFM to synthesize their training data, which is unrealistic for real-world tasks of underwater image enhancement.

Compared with these methods mentioned above, our underwater image dehazing model combines the merits of non-IFM and IFM-based methods, which contains not only the natural appearance and high contrast but also global color cast removal for diverse underwater images. The main contributions of this work can be summarized as follows:

1) We propose an adaptive color correction algorithm using parameters estimation of Gaussian model, providing redistribution of histograms on each RGB color channel based on a linear transformation. The significant peak deviation of histogram distributions of the original underwater images can be effectively modified to concentrated area among RGB channels and the histogram are characterized by more broad range of distribution after color correction.

2) With weighted combination of gradient maps in HSV color space and absolute difference of intensity of grayscale images, the background light can be accurately selected from the location of the darkest pixel in this map, which effectively avoids the influence of white or bright regions that challenges existing methods. To our best knowledge, it is the first algorithm of background light estimation that based on the superposed map for inference.

3) We propose a piece-wise affine transform applied for stretching the transmission map, which aims at revealing more details and valuable information and increasing contrast of the scene radiance.

4) As a thorough work of underwater image enhancement, extensive experiments on diverse underwater datasets show that our method can effectively eliminate color cast and the haze of the original underwater images, which thus demonstrated better robustness and higher generalization of our method compared with the state-of-the-arts.

3 Proposed method

As shown in Fig. 1, we first introduce an adaptive color correction algorithm based on maximum likelihood estimation of Gaussian parameters for a wide range of underwater images. Then, we propose a novel approach for effective background light estimation. And the enhanced transmission map is obtained by a piece-wise affine transform for scene radiance restoration. At last, the dehazing result can be calculated by IFM. As follows, we will introduce these key algorithms in our method.

3.1 Adaptive color correction

Color correction for underwater images primarily aims at balancing undesired color distortions caused by the selective absorption theory of water, i.e., the red light is much easier to be absorbed than the green and blue light, and the shorter wavelengths of green and blue light will be much more easily scattered than the longer wavelength of the red light [8]. Therefore, underwater images often show greenish or bluish tone in most cases. According to the observations in [30], the red and blue channels are supposed to be compensated at each pixel location. However, it is insufficient to compensate just red and blue channels when the green channel is noticeably attenuated (see Fig. 2. (b1), for display, the global linear contrast stretching is performed by clipping 0.1‰ of the pixel values in the shadows and 0.1% in the highlights [41]). Thus, we further take the green compensation into consideration for a more natural appearance as follows:

$$I_{RC}(x,y) = I_R(x,y) + (\bar{I}_G - \bar{I}_R)(1 - I_R(x,y))I_G(x,y), \quad (1)$$

$$I_{GC}(x,y) = I_G(x,y) + (\bar{I}_B - \bar{I}_G)(1 - I_G(x,y))I_B(x,y), \quad (2)$$

$$I_{BC}(x,y) = I_B(x,y) + (\bar{I}_G - \bar{I}_B)(1 - I_B(x,y))I_G(x,y), \quad (3)$$

where $\bar{I}_R$, $\bar{I}_B$, and $\bar{I}_G$ represent the mean value of red, green, and blue channel respectively.

In order to further reduce discrepancy of distribution among color channels, we employ the maximum likelihood estimation (MLE) for unknown Gaussian parameters determining RGB color histogram modification after color compensation. The probability density function of Gaussian distribution can be commonly defined as follows:

$$f(x) = \frac{1}{\sqrt{2\pi}\sigma} \exp\left(-\frac{(x-\mu)^2}{2\sigma^2}\right), \quad (4)$$

where μ and σ^2 represent mean and variance of Gaussian

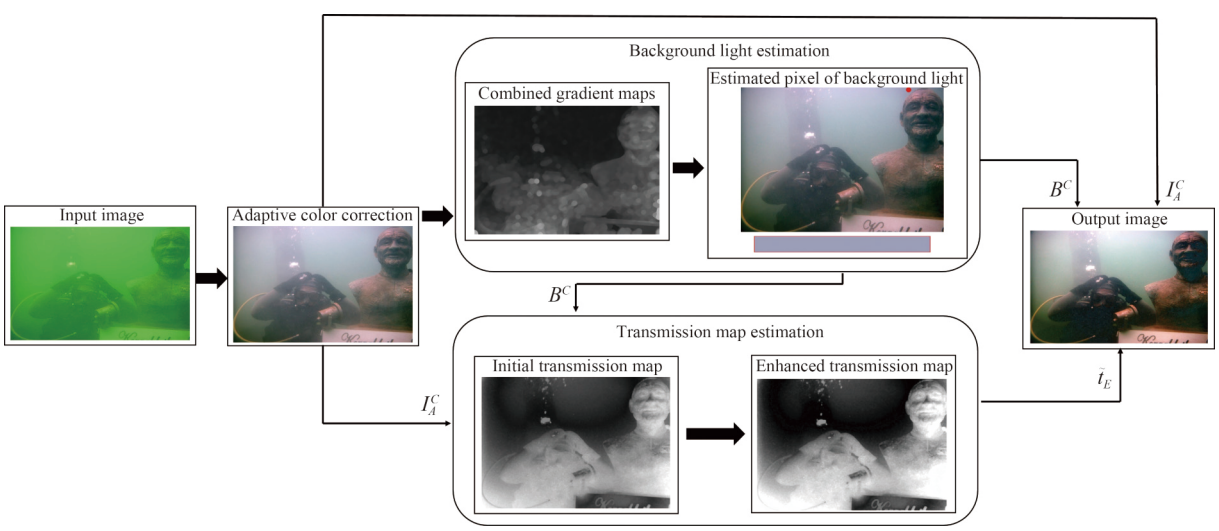

Fig. 1 The flowchart of the proposed method

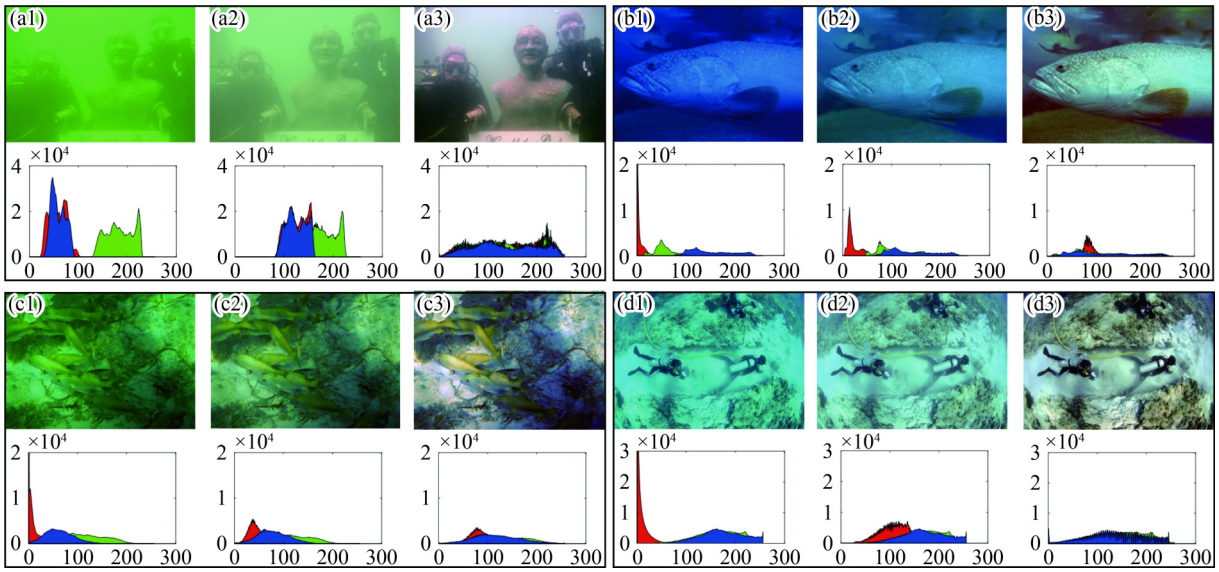

Fig. 2 Adaptive color correction for underwater images. (a1) Greenish image. (b1) Bluish image. (c1) Greenish-blue image. (d1) Bluish-green image. (a2), (b2), (c2) and (d2) Color compensation using red, green, and blue channels. (a3), (b3), (c3) and (d3) The results of our proposed adaptive color correction. The corresponding RGB histograms are shown under each result

distribution.

Then we can obtain the parameters of Gaussian model via maximizing the likelihood of a given set of observations of each color channel. The MLE of μ and σ^2 can be denoted as follows:

$$\mu = \frac{1}{N}\sum_{n=1}^{N} x_n, \tag{5}$$

$$\sigma^2 = \frac{1}{N}\sum_{n=1}^{N} (x_n - \mu)^2, \tag{6}$$

where N is the number of pixels and x_n is the grayscale value of the nth pixel in each channel.

According to the results of MLE, the distribution of color histograms can be adaptively adjusted as:

$$I_A^R = 0.5 + (\max I_{RC} - \min I_{RC})\left(\frac{\sigma_{GC}}{\sigma_{RC}}\right)(I_{RC} - \mu_{RC}), \tag{7}$$

$$I_A^G = 0.5 + (\max I_{GC} - \min I_{GC})\left(\frac{\sigma_{BC}}{\sigma_{GC}}\right)(I_{GC} - \mu_{GC}), \tag{8}$$

$$I_A^B = 0.5 + (\max I_{BC} - \min I_{BC})\left(\frac{\sigma_{GC}}{\sigma_{BC}}\right)(I_{BC} - \mu_{BC}), \tag{9}$$

where μ_{RC}, μ_{GC}, μ_{BC}, σ_{RC}, σ_{GC}, and σ_{BC} represent mean and standard deviation of red, green and blue channel after color compensation, I_A^R, I_A^G, and I_A^B denote results of adaptive color correction on different color channels respectively. According to relative degree of dispersion between red and green in Eq. (7), green and blue in in Eq. (8), blue and green in Eq. (9), the coefficients $(\max I_{x1} - \min I_{x1})\left(\frac{\sigma_{x2}}{\sigma_{x1}}\right)$ $x1, x2 \in \{RC, GC, BC\}$ are in the interval [0, 1] to control the ratio of the intensity mapping, while $(\max I_{x1} - \min I_{x1})\left(\frac{\sigma_{x2}}{\sigma_{x1}}\right)\mu_{x1}$ $x1, x2 \in \{RC, GC, BC\}$ is employed to control the shifting range from normalized median 0.5. As for most underwater images with attenuated red channel, especially when it comes to severe attenuation, σ_{RC} is often smaller than σ_{GC} and μ_{RC} is generally the smallest in RGB color channels. Therefore, the relatively smaller red channel values tend to be mapped to larger value in a wider range.

3.2 Underwater image dehazing

Our proposed underwater image dehazing method is comprised of two main parts: background light and transmission map estimation, where the corresponding parameters of IFM are estimated for solving the inverse problem. As shown in Fig. 3, the simplified underwater imaging model employed in most existing techniques [41,42] can be described as Eq. (10). The transmission map describes the proportion of the scene radiance reaching the camera without scatter or absorption and the image intensity of each pixel (x,y) in each color channel includes two components: background light and attenuated signal.

$$I_A^c(x,y) = J^c(x,y)t^c(x,y) + B^c(1 - t^c(x,y)), \tag{10}$$

where $c \in \{r,g,b\}$, $I_A(x,y)$ denotes the observed intensity at pixel (x,y) after adaptive color correction, the scene radiance $J(x,y)$ blended with the transmission map $t(x,y)$ describes the direct attenuation, while the second term related to the background light B^c accounts for remaining portion.

3.2.1 Background light estimation

According to the traditional DCP-based method, $I_{A-DCP}^{RGB}(x,y) = \min\limits_{(x,y)\in\Omega(i,j)}\left\{\min\limits_{c\in\{R,G,B\}} I_A^c(x,y)\right\}$, where $I_A(x,y)$ represents the image processed by adaptive color correction, can provide the information of scene depth for a hazy image due to effect of scattered light, i.e., the foreground (close scene pixels) generally contains more dark pixels while the background (far

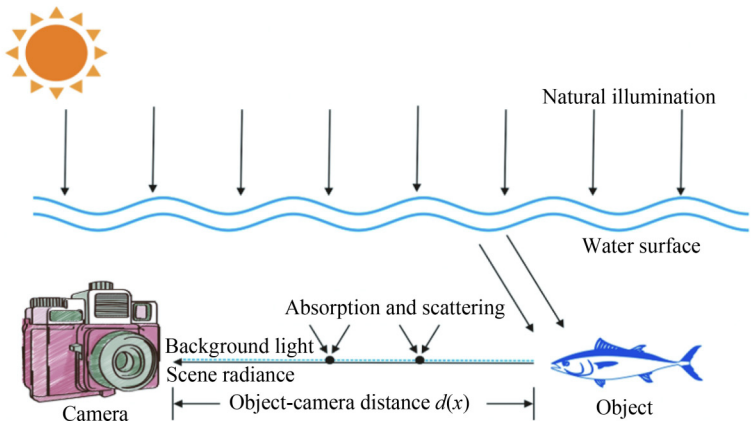

Fig. 3 Underwater imaging model

scene pixels) lacks dark pixels under appropriate lighting conditions. Thus, the background light B^c can be selected from one of the top 0.1% brightest scene pixels in the dark channel and the pixel with the highest intensity among these candidates can be used for background light estimation. However, it is inaccurate to estimate the background light via the DCP when it comes to a bright object, foreground or highlight region captured in underwater images. As can be seen from Fig. 4, the red dots denote locations where background light is estimated by means of traditional dark channel, while the yellow dots represent the background light locations of our proposed method. Apparently, traditional DCP leads to incorrect background light selection due to the bright area.

In general, we can observe that objects or regions near the camera tend to show more details including texture and edge information, while far scene points are likely to have smoother regions and thus smaller gradients than close scene points due to the effect of forward and backward scattering in underwater environment. Therefore, the background light can be estimated according to inference of the scene depth using a gradient map under the assumption that scene depth is uniform in a small local patch [29]. Inspired by this observation, we use gradient maps of each component in HSV color space containing complementary information of edges combined with the absolute difference of intensity values to accurately estimate the background light.

The gradient maps of H, S, and V components are computed as $M_{HSV}(x,y) = \sqrt{M_h(x,y)^2 + M_v(x,y)^2}$ in HSV color space respectively (Figs. 5. (a2)−(a4)), where M_h and M_v signify horizontal and vertical 3 × 3 Roberts operators. While Fig. 5 (b1) shows the absolute difference of intensity values of gray-scale image, which is computed as $\tilde{M}_G(x,y) = |0.4 - Gray(I)|$, with the purpose of excluding those very bright or dark regions that can hardly be detected due to smoothness. As can be observed from Figs. 5 (b2)−(b4), a group of modified gradient maps $\tilde{M}_{HSV}(x,y)$ are estimated by dilating $M_{HSV}(x,y)$ followed by filling holes, which aims at expanding regions containing detected edge and texture information. The integrated map of background light estimation consists of four parts that are combined with appropriate weights as follows:

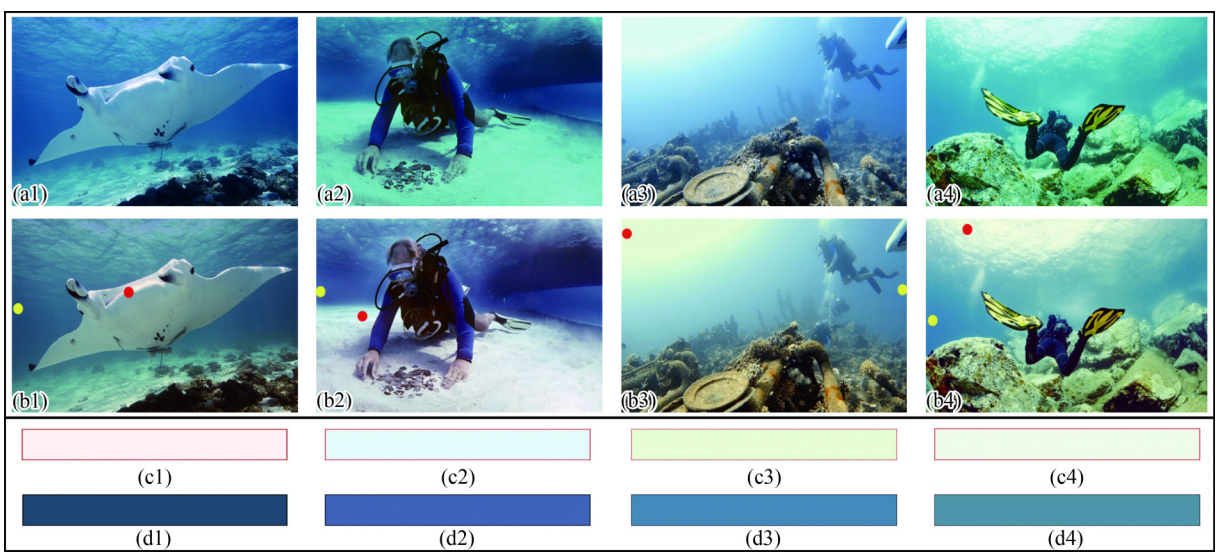

Fig. 4 Background light estimation using results of the proposed adaptive color correction. (a1)−(a4) Original images. (b1)−(b4) The locations of estimated background light (red and yellow dots signify DCP-based and our proposed methods respectively). (c1)−(c4) RGB color of the corresponding red dots. (d1)−(d4) RGB color of the corresponding yellow dots

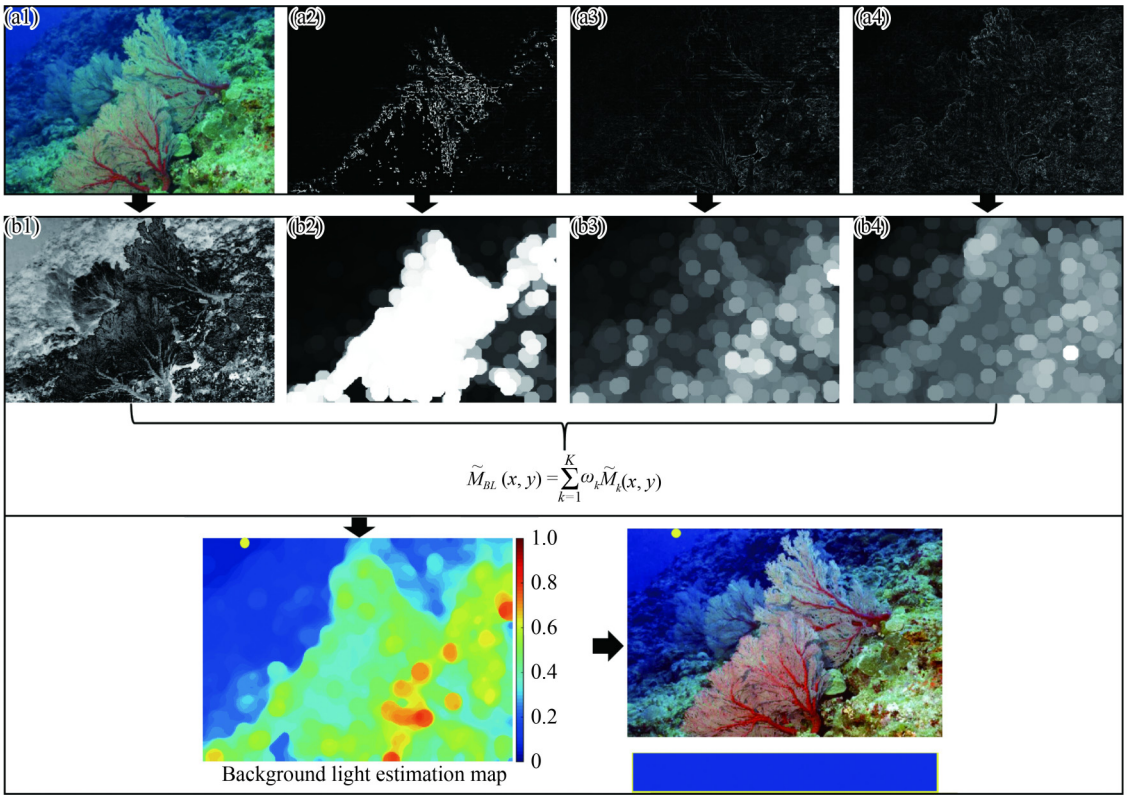

Fig. 5 Background light estimation map. (a1) Original images. (a2)−(a4) The gradient maps of H, S, V component in HSV color space. (b1) Absolute difference map. (b2)−(b4) The modified gradient maps of (a2)−(a4) respectively. The yellow dot denotes the location of estimated background light in bottom estimation map

$$\tilde{M}_{BL}(x,y)=\sum_{k=1}^{K}\omega_k\tilde{M}_k(x,y), \tag{11}$$

where $K=4$ and the weighted coefficients are empirically selected as $\omega_1=0.1$, $\omega_2=0.4$, $\omega_3=0.4$, and $\omega_4=0.1$. In order to obtain the final vector B^c, it will be selected from one location of the darkest pixels (0.01%) in the integrated map.

3.2.2 Transmission map estimation and enhancement

As described in Eq. (10), it can be rewritten as:

$$t^c(x,y)\left|J^c(x,y)-B^c\right|=\left|I_A^c(x,y)-B^c\right|,\quad c\in\{r,g,b\}. \tag{12}$$

According to the observation that closer scene points consist more of scene radiance and less of background light while farther scene point consists less of scene radiance and more of background light [29], both sides are divided by $\max\{B^c,1-B^c\}$ and the maximum operators are applied to Eq. (12), so that the transmission map estimation can be described as:

$$\begin{aligned}&\max_{c,(x,y)\in\Omega(i,j)}\left(\frac{t^c(x,y)\left|J^c(x,y)-B^c\right|}{\max\{B^c,1-B^c\}}\right)\\&=\max_{c,(x,y)\in\Omega(i,j)}\left(\frac{\left|I_A^c(x,y)-B^c\right|}{\max\{B^c,1-B^c\}}\right).\end{aligned} \tag{13}$$

Within 15×15 local patch $\Omega(x,y)$, more than 75% of pixels in 60 natural degradation-free images can be found that $\max_{c,(x,y)\in\Omega(i,j)}\left(\frac{\left|J^c(x,y)-B^c\right|}{\max\{B^c,1-B^c\}}\right)\approx 1$ [6], so that:

$$\tilde{t}(x,y)\approx\max_{c,(x,y)\in\Omega(x,y)}\left(\frac{\left|I_A^c(x,y)-B^c\right|}{\max\{B^c,1-B^c\}}\right). \tag{14}$$

In order to enhance contrast of recovery, the piece-wise affine transform [43] is applied for stretching the transmission map computed in Eq. (14), the transmission map is reshaped as an array of M numeric values between [0, 255], [0, $V_{\min-}$], [$V_{\min-}$, $V_{\min}$], [$V_{\min}$, $V_{\max}$], [$V_{\max}$, $V_{\max+}$] and [$V_{\max+}$, 255] are five possible ranges, which can be defined as follows:

$$\tilde{t}_E(x,y)=\begin{cases}0, & \tilde{t}(x,y)<V_{\min-},\\ 255\times0.05\times\dfrac{(\tilde{t}(x,y)-V_{\min-})}{(V_{\min}-V_{\min-})}, & V_{\min-}\leqslant\tilde{t}(x,y)<V_{\min},\\ 255\times\dfrac{(\tilde{t}(x,y)-V_{\min})}{(V_{\max}-V_{\min})}, & V_{\min}\leqslant\tilde{t}(x,y)\leqslant V_{\max},\\ 255\times\left(0.99\times\left(1+\dfrac{\tilde{t}(x,y)-V_{\max}}{V_{\max+}-V_{\max}}\right)\right), & V_{\max}<\tilde{t}(x,y)\leqslant V_{\max+},\\ 255, & \tilde{t}(x,y)>V_{\max+},\end{cases} \tag{15}$$

where V_{max} and V_{min} denote the value of the $((1-p\%)\times M+1)$th and the $(p\%\times M)$th pixel respectively, while V_{max+} and V_{min-} denote the pixel value which is ranked top 20% between V_{max} and 255 and the lowest 20% between 0 and V_{min}, p is set to be 0.1.

Now that the background light and enhanced transmission map are estimated (see Fig. 6), the clear scene radiance can be computed by Eq. (16). In order to avoid less natural appearance and too much noise, t_0 is set to be 0.75.

$$J^c(x,y)=\frac{I_A^c(x)-B^c}{\max(\tilde{t}_E(x,y),t_0)}+B^c, c\in\{r,g,b\}. \quad (16)$$

4 Experimental results and discussion

In order to verify the effectiveness of our proposed method, color accuracy test is firstly conducted on seven standard underwater images taken in a swimming pool with Macbeth Color Checker. These images were taken with seven different cameras containing various kinds of color distortion provided by [34]. Then, we further perform experiments on more challenging underwater scenes provided by Berman et al. [27], which also contain color charts and were taken in different locations with varying water properties.

In the second part of experiments, we compare the proposed method with six underwater image enhancement methods (i.e., Drews 2016 [5], Fu 2017 [33], Peng 2017 [26], Peng 2018 [29], Gao2019 [44], Fu 2020 [2]). Note that we mainly compare with traditional methods for a fair comparison. However, we also compare with a recent deep learning-based method [2] which is a strong learning-based baseline. The subjective and objective evaluations including full-reference (PSNR, SSIM, MSE, and HCC [45]) and non-reference metrics (UCIQE [46] and Image Entropy) are employed to evaluate the performance of different methods on Underwater Image Enhancement Benchmark (UIEB) [1], which consists of 890 real-world underwater images. In order to provide additional evidence of the effectiveness of our dehazing method, we carry out the third part of experiments on challenging-60 of UIEB dataset and high turbid data. It is worth noting that [44] directly provides a limited number of results and results of [2] are implemented with Python3.5 on a Linux PC, while other tested algorithms are implemented with Matlab R2018a on a Windows PC.

4.1 Color accuracy test

The standard color checker including 24 patches in a 4×6 grid is usually employed for testing robustness of various methods. Therefore, our first experiment is designed to demonstrate the effectiveness and robustness of our adaptive color correction (ACC) method, and the results are visualized in Fig. 7. There are seven different testing images taken with Canon D10, Olympus T8000, Olympus T6000, FujiFilm Z33, Pentax W80, Pentax W60 and Panasonic TS1 respectively. In addition to classic color constancy methods including Shades of Grey [47], Max RGB [48], Grey World [49], and Grey Edge [50], we compare our method with Gao 2019 [44] and Fu 2020 [2], which are based on biologically inspired adaptive retinal mechanisms and deep global-local network architecture respectively.

As can be seen in the first row, all the original images suffer from extreme color distortion and low contrast. Those classic color constancy methods and Gao 2019 are not capable of accurately removing the distorted color, which are displayed from the second to the sixth rows. By contrast, Fu 2020 is able to correct color distortion for most testing underwater images except for the last one taken with Panasonic TS1. While our proposed method can effectively address such issues and obtain relatively genuine color and natural appearance by color compensation and adaptive correction without complex and time-consuming network training with massive training data.

In order to further evaluate our dehazing method and compare it to other five methods, we employed more challenging Berman dataset. From Fig. 8, the original images taken in different diving spots with varying water properties contained three different color charts that enclosed with red rectangle and close-up views of the corresponding regions of results are clearly displayed. In addition to obtaining better

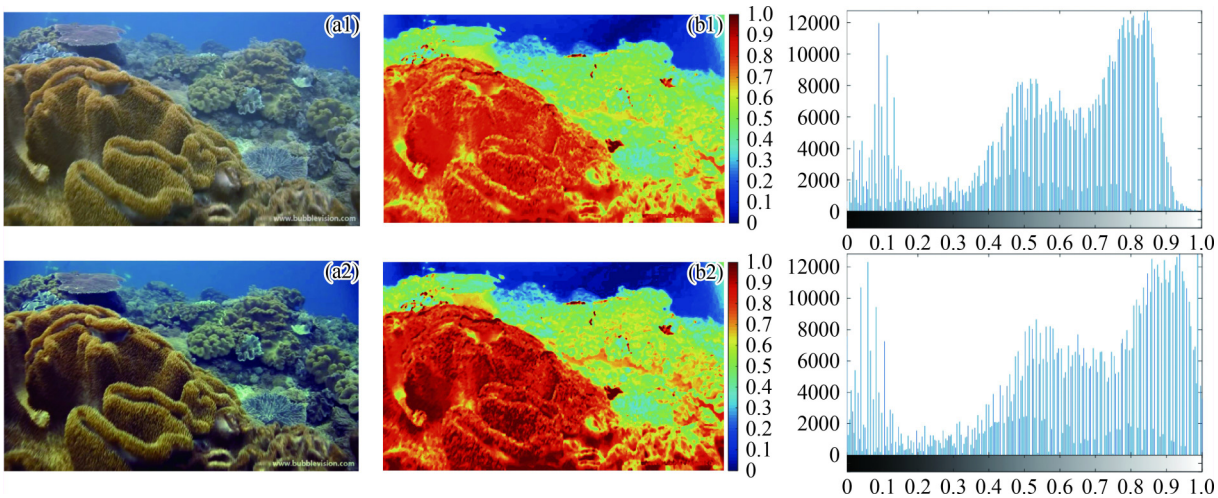

Fig. 6 Enhanced transmission map using the piece-wise affine transform. The original image is shown in (a1). The result of adaptive color correction is shown in (a2). The result of transmission map estimation when using Eq. (14) is shown in (b1). While utilizing our piece-wise affine transform generates higher contrast, as shown in (b2). And the corresponding histograms of transmission map are displayed on the right side

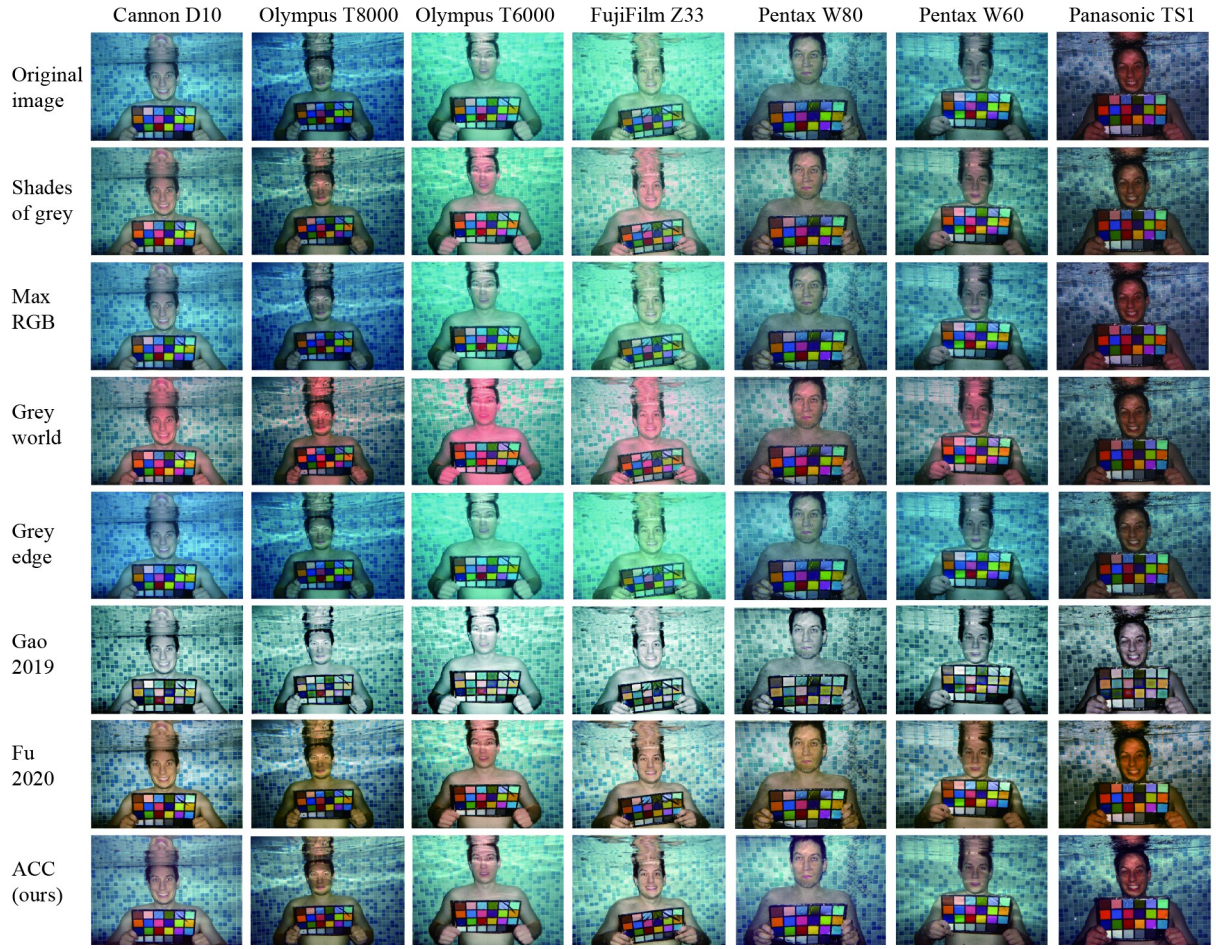

Fig. 7 Comparison to classic color constancy, Gao 2019 [44] and Fu 2020 [2] approaches. The original images taken with seven different cameras are shown in the first row. The result of our proposed method (ACC) are shown in the last row

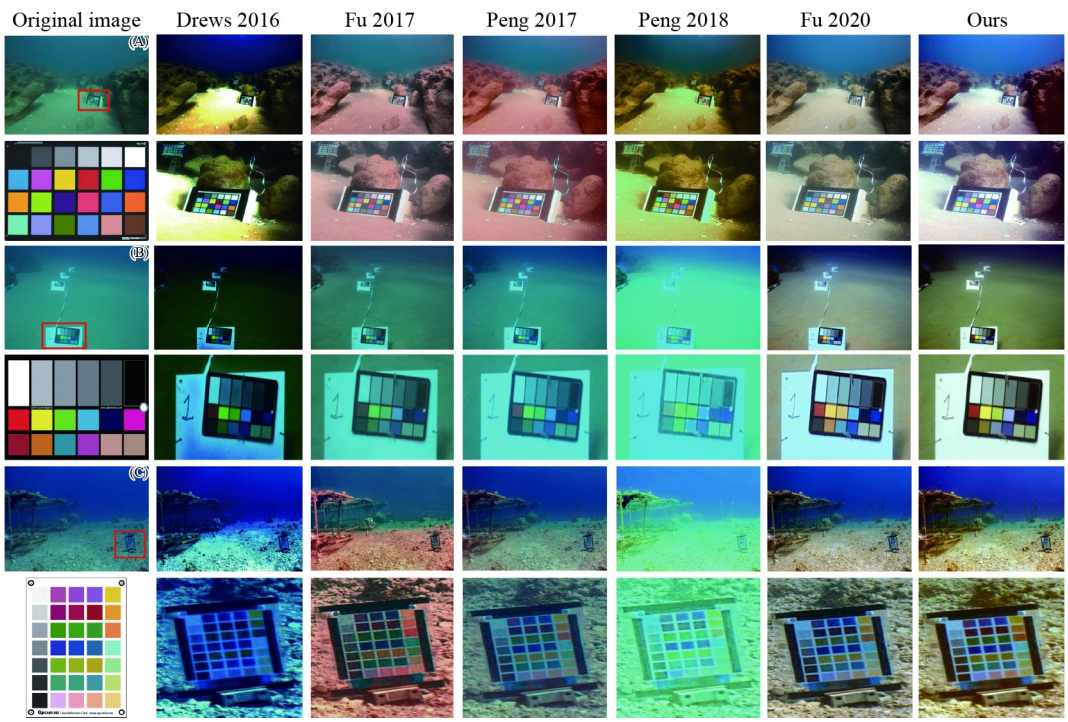

Fig. 8 Qualitative comparisons on Berman dataset. The original images taken in different locations with varying water properties contain three different color charts (red rectangle) and the corresponding standard color charts are shown below. From left to right are original images, the results of Drews 2016 [5], Fu 2017 [33], Peng 2017 [26], Peng 2018 [29], Fu 2020 [2], and our proposed method

contrast and visibility, both Fu 2020 and our approach can provide the relatively accurate color correction and thus obtain more natural appearance compared with Drews 2016, Fu 2017, Peng 2017, and Peng 2018, respectively. Next, Table 1 reports the quantitative results using non-reference metrics in terms of UCIQE and Entropy on scene A, B and C. The average scores of our method perform the best across all metrics followed by Fu 2020, which are marked in red and blue respectively and consistent with subjective observation in Fig. 8. As for different underwater scenes with color charts in color accuracy test, our approach provides better results in terms of both subjective and objective evaluations and thus has better robustness.

4.2 Experimental results on 890 images of UIEB dataset

In this part, a large UIEB dataset, 890 of which have the corresponding reference images and 60 of which as challenging data, is employed to verify the robustness of our underwater image dehazing method. Because the underwater images have various degradation issues, such as diverse degrees of color shift and contrast decrease. Thus, a comprehensive study will be carried out for several state-of-the-art underwater image enhancement or restoration methods both qualitatively and quantitatively.

To begin with, the underwater images are selected from extreme greenish to bluish appearance which covers most types of color casts. In Fig. 9, we can notice that the outputs of Drews 2016, Peng 2017, and Peng 2018 are visually different from that of other approaches, since color casts are hard to be effectively removed by these algorithms, particularly the first and sixth-row images with extreme greenish and bluish tone. While the results of Fu 2017 and Gao 2019 show low degree of saturation and contrast for most testing images. By comparison, the visual effects of the outputs of Fu 2020 and our

Table 1 Results of non-reference metrics in terms of UCIQE and Entropy. The best results are highlighted in red and the second best results are marked in blue

Method	Non-reference metrics							
	UCIQE↑				Entropy↑			
	Scene A	Scene B	Scene C	Average	Scene A	Scene B	Scene C	Average
Drews 2016 [5]	0.6959	0.5485	0.6691	0.6212	6.7810	4.4696	6.0323	5.7610
Fu 2017 [33]	0.6080	0.4380	0.6599	0.5686	7.2340	5.3133	6.7848	6.4441
Peng 2017 [26]	0.6355	0.4663	0.5772	0.5597	7.3876	5.1223	6.4637	6.3245
Peng 2018 [29]	0.6536	0.3771	0.4791	0.5033	7.3589	4.9163	6.3101	6.1951
Fu 2020 [2]	0.6428	0.5867	0.6542	0.6279	7.1995	6.4094	6.7895	6.7995
Ours	0.6883	0.6016	0.6803	0.6567	7.7000	6.8094	7.1749	7.2281

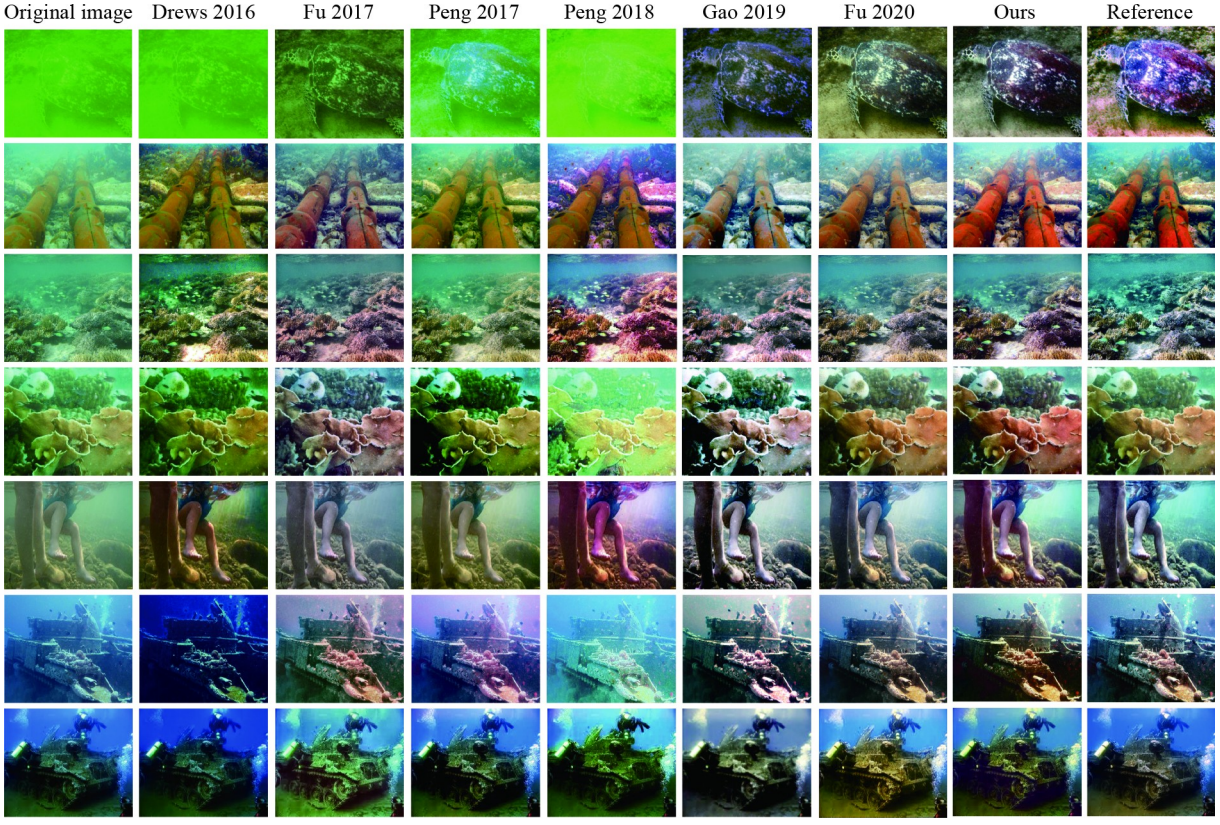

Fig. 9 Qualitative comparisons on UIEB dataset (890 images). From left to right are original images, the results of Drews 2016 [5], Fu 2017 [33], Peng 2017 [26], Peng 2018 [29], Gao2019 [44], Fu 2020 [2], our proposed method and reference images

Table 2 Quantitative evaluation of results on UIEB dataset. The best results are highlighted in red and the second best results are marked in blue

Method	Full-reference metrics				Non-reference metrics	
	PSNR↑	SSIM↑	MSE($\times 10^3$)↓	HCC↑	UCIQE↑	Entropy↑
Drews 2016 [5]	12.4737	0.6173	4.3301	0.1631	0.5896	6.5381
Fu 2017 [33]	19.4887	0.8421	1.1258	0.4277	0.5761	7.2849
Peng 2017 [26]	17.9254	0.7821	1.5937	0.3334	0.5972	7.1622
Peng 2018 [29]	13.4894	0.7306	3.6482	0.1105	0.5947	7.1338
Fu 2020 [2]	21.3105	0.8779	0.6567	0.3577	0.6363	7.3254
Ours	19.9451	0.8466	0.8545	0.4290	0.6454	7.6090

proposed method illustrate the high robustness under different underwater conditions.

Moreover, four commonly-used metrics (PSNR, SSIM, MSE and HCC) as full-reference evaluation can provide quantitative image quality assessment as 890 images in UIEB dataset contain the corresponding references, while UCIQE and Entropy as non-reference evaluation are employed for underwater image quality assessment. It should be noted here that PSNR, SSIM, HCC, UCIQE and Entropy, the higher, the better while the MSE, the lower, the better. As can be seen from Table 2, except for HCC, Fu 2020 achieves the best among the competitors in terms of full-reference evaluation, while our method achieves promising results, ranking the second best marked in blue. It is primarily because the first 700 images of the UIEB dataset are directly used for training their network by Fu 2020. As a supervised deep learning-based method, it is more likely to obtain higher PSNR and SSIM when 890 images of UIEB dataset are used for full-reference evaluation. On the contrary, our method performs best on non-reference evaluation, which are consistent with the qualitative results as shown in Fig. 9. A higher UCIQE value denotes that the image has better balance among the chroma, contrast and saturation, while higher entropy value indicates more information contained in the image. As for HCC, it is specifically presented for assessing the performance of color restoration based on histogram correlation coefficient, and higher values signify more histogram correlation between the results and reference images.

4.3 Experimental results on challenging-60 of UIEB dataset and high turbid data

In addition to 890 underwater images, we conduct experiments on the rest 60 challenging data of UIEB dataset and 30 high turbid underwater images collected by ourselves to validate the generalization of the proposed method. Sometimes underwater imaging systems suffer from so special environment that the images taken there are entirely distinct from common tone or hazy appearance, which can be observed as the original images in Figs. 11 and 12. It should be noted here that all the high turbid data are not contained in UIEB dataset and were taken in the natural underwater environment, which was not designed by man-made for specific experimental purpose.

We resort to an effective metric which estimates the degree of haziness based on the transmission component and wavelet transform (TCWT) [51] to define high turbid data, and higher score of TCWT represents better visibility. As shown in Fig. 10, the average score of TCWT of the original 890 images on

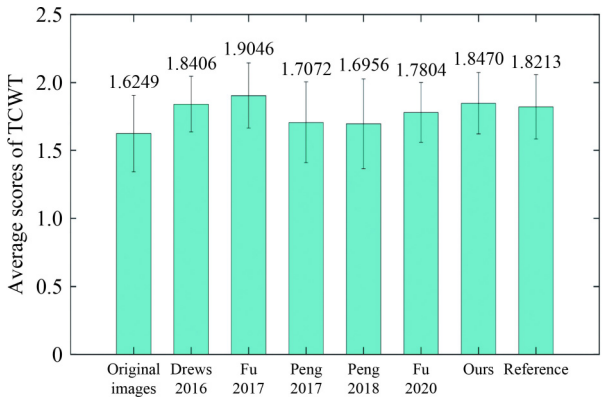

Fig. 10 Average scores of TCWT. From left to right are the results of original images (*Std* = 0.2822), Drews 2016 [5] (*Std* = 0.2051), Fu 2017 [33] (*Std* = 0.2401), Peng 2017 [26] (*Std* = 0.2978), Peng 2018 [29] (*Std* = 0.3305), Fu 2020 [2] (*Std* = 0.2205), our proposed method (*Std* = 0.2265), and reference (*Std* = 0.2375)

UIEB dataset ranks last among these methods, which is coherent with subjectively visual quality. It is obvious that all the methods for enhancement or restoration yield significant improvement in terms of TCWT. Since the average and standard deviation of original images are $\mu = 1.6249$ and $\sigma = 0.2822$ respectively, we define that high turbidity exists in an underwater image when TCWT score is less than 1.3427 $(\mu - \sigma)$ according to Gaussian distribution, while just slight turbidity exists when TCWT score is more than 1.9071 $(\mu + \sigma)$. The average and standard deviation of TCWT score of high turbid dataset are $\mu = 1.1981$ and $\sigma = 0.1074$ respectively.

Figures 11 and 12 show visual results from UIEB dataset (challenging-60 images) and high turbid data. As can be seen, the methods of Drews 2016, Peng 2017, and Peng 2018 fail to remove original color deviation. The results of Fu 2017 tends to slightly correct distorted colors while yields low contrast and visibility. By contrast, our proposed method and Fu 2020 are able to well correct color distortion and effectively remove haze on different kinds of challenging real-world underwater scenes with naturalness preservation. Furthermore, our method still achieves the best performance on both UCIQE and Entropy metrics from Table 3. Both qualitative and quantitative evaluation demonstrate the validity of our color correction and dehazing method on more challenging tasks.

4.4 Application test

To further verify the effectiveness of our proposed method, we perform experiments on computer vision applications. Harris

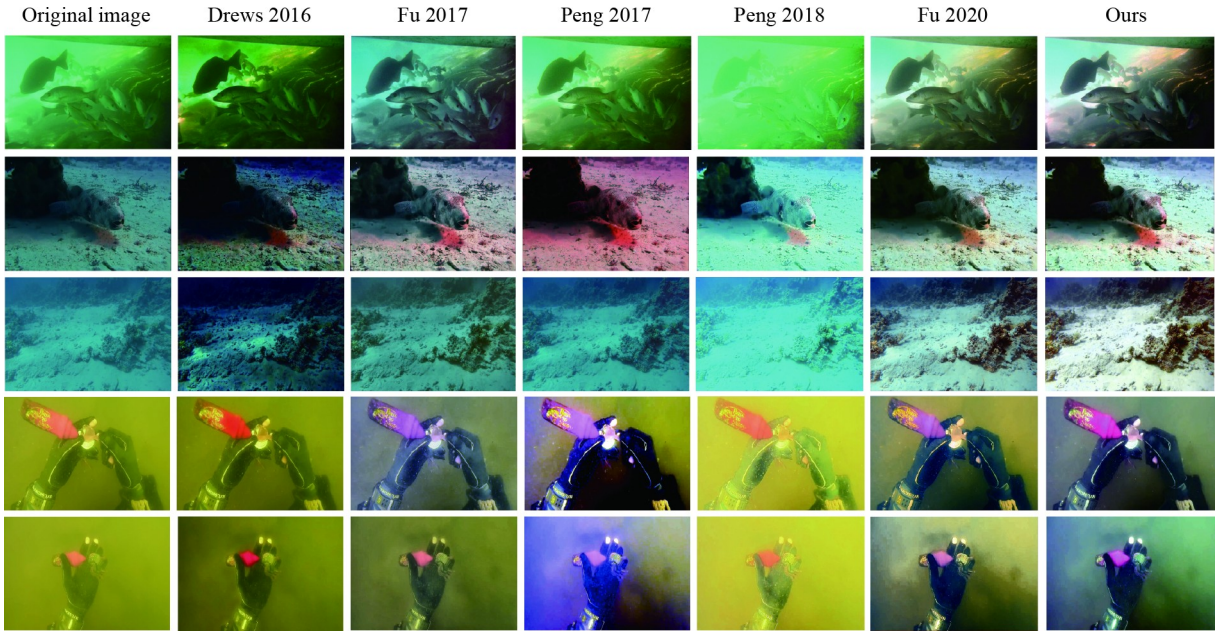

Fig. 11 Qualitative comparisons on UIEB dataset (challenging-60 images). From left to right are original images, the results of Drews 2016 [5], Fu 2017 [33], Peng 2017 [26], Peng 2018 [29], Fu 2020 [2], and our proposed method

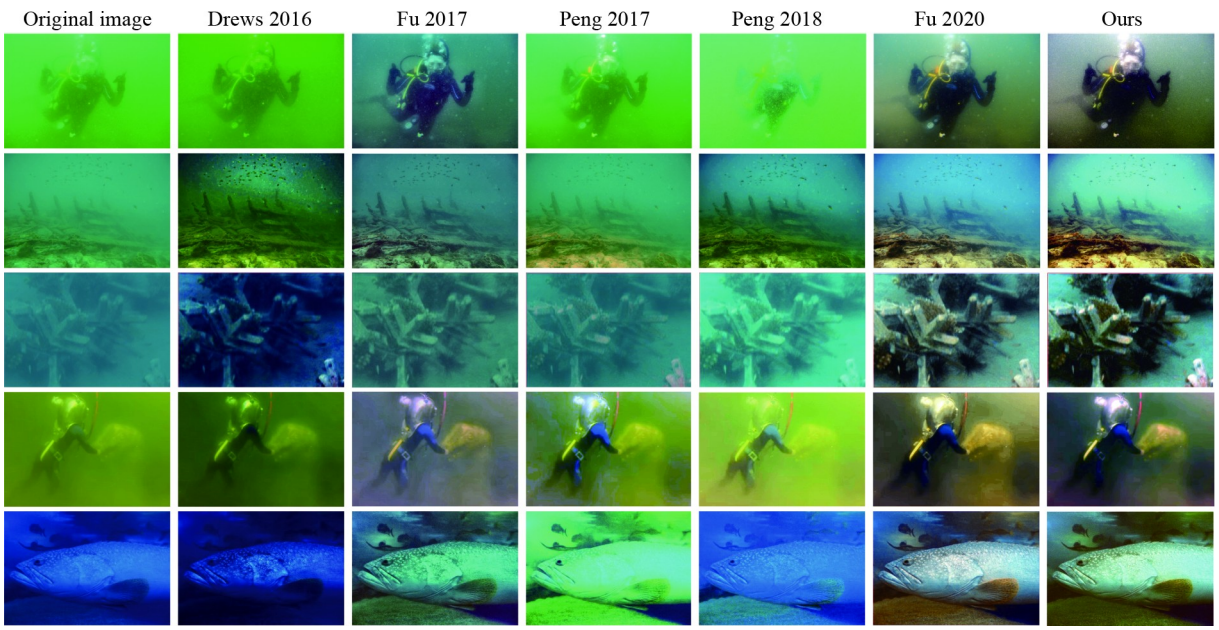

Fig. 12 Qualitative comparisons on high turbid data. From left to right are original images, the results of Drews 2016 [5], Fu 2017 [33], Peng 2017 [26], Peng 2018 [29], Fu 2020 [2], and our proposed method

Table 3 Quantitative evaluation of results on UIEB dataset (challenging-60 images) and high turbid data. The best results are highlighted in red and the second best results are marked in blue

Method	Non-reference metrics					
	UCIQE↑			Entropy↑		
	Challcnging-60	High-turbid-30	Average	Challcnging-60	High-turbid-30	Average
Drews 2016 [5]	0.5309	0.5049	0.5179	5.8613	5.5584	5.7099
Fu 2017 [33]	0.5445	0.5128	0.5287	6.9774	6.6771	6.8273
Peng 2017 [26]	0.5830	0.5104	0.5467	6.9195	6.5152	6.7174
Peng 2018 [29]	0.5589	0.5129	0.5359	6.8922	6.3590	6.6256
Fu 2020 [2]	0.6028	0.6072	0.6050	6.9457	7.0245	6.9851
Ours	0.6271	0.6170	0.6221	7.3745	7.5897	7.4821

corner detection [52] and SIFT feature matching [53] are firstly adopted to find interest points and correspondences between underwater image pairs which have similar scenarios. Then, salient region detection [54] is utilized to extract key information of the target scene. According to the experimental results in Fig. 13, the interest points that can be found as well as the number of valid matched features are significantly increased in the dehazing image pairs. Moreover, Figure 14 shows that our dehazing results achieve better performance of salient region detection.

4.5 Failure cases and discussion

Two failure examples of our dehazing method are shown in Fig. 15. Compared with other methods, our proposed approach is capable of removing color distortion but amplifies lighting areas when the scenes exhibit extreme non-uniform illumination conditions caused by active light sources, yielding locally too bright visual effects. The global color compensation and histogram modification cannot reduce effects of overexposure, and subsequent wrong background light estimation may cause our method to fail to process underwater images with active light sources.

4.6 Ablation study

To examine the effect of correct background light estimation in our proposed method, we conduct ablation study on UIEB dataset and replace the integrated map with DCP-based background light estimation (w/o ours) for comparison. It can be seen from Fig. 16, the results of our method can provide more natural appearance and genuine color while the results with wrong estimation of background light show detail loss and color distortion. In addition to subjective observation from Fig. 16, our method still achieves the better performance on PSNR, SSIM, UCIQE and Entropy metrics respectively. As can be seen from Table 4, the higher UCIQE and image entropy indicate that our proposed integrated map for background light estimation introduces a better human visual perception and more information contained in that image.

5 Conclusion

In this paper, we proposed adaptive color correction and robust scattering removal for underwater image enhancement. Using color compensation and MLE-based color histogram modification, we demonstrate that the proposed method can reduce discrepancy of distribution among color channels and

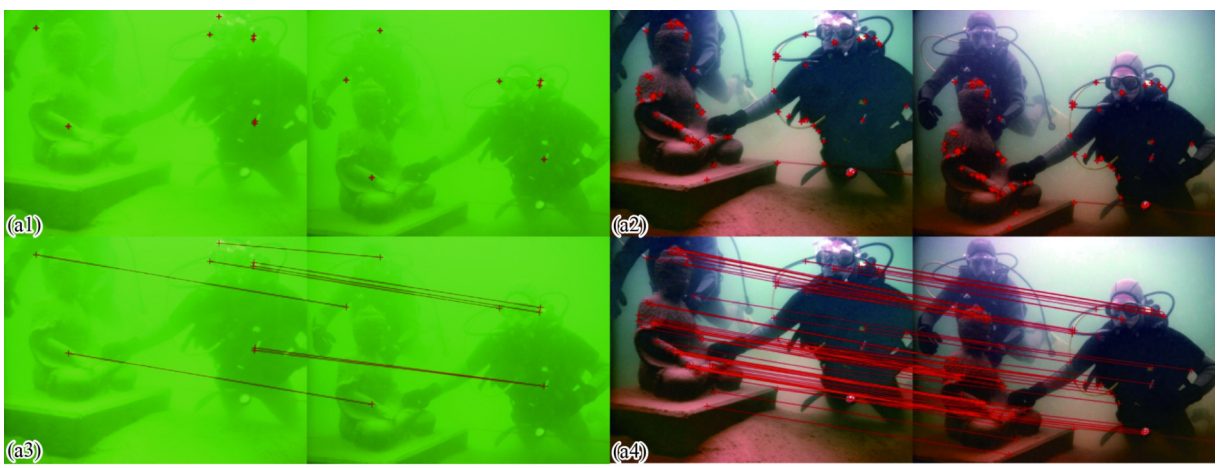

(a)

(b)

Fig. 13 Interest points detection and SIFT feature matching. For the left-side pair ((a1) and (a3), (b1) and (b3)), Harris corner detections only find 8 and 2 interest points that can be correctly matched when using SIFT features based on original image pairs. For the right-side pair ((a2), (a4), (b2), (b4)), there are 80 and 90 interest points found and correctly matched when using Harris corner detection and SIFT feature matching respectively based on dehazing image pairs. (a) The first pair of underwater images; (b) The second pair of underwater images

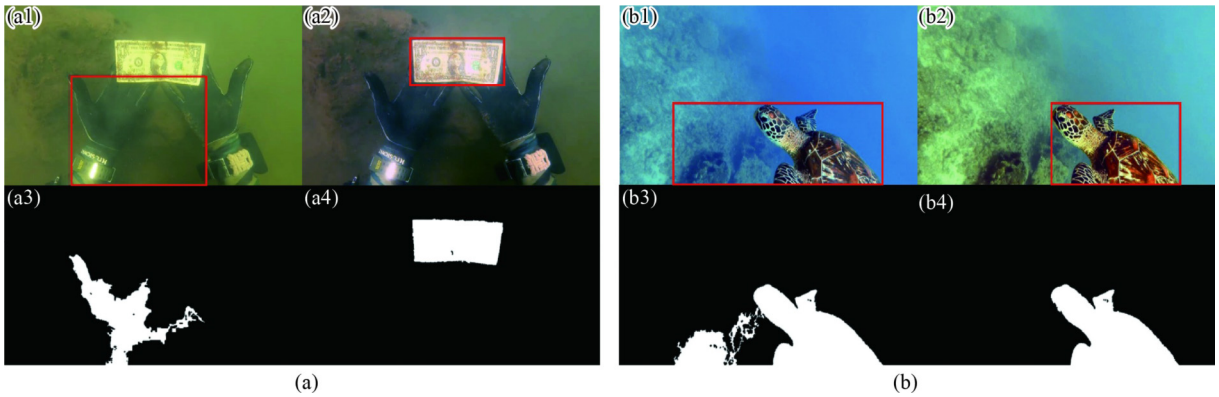

Fig. 14 The visual comparison of salient region detection. Compared with the left-side pair ((a1) and (a3), (b1) and (b3)), salient regions can be more accurately detected using the results of our dehazing method ((a2) and (a4), (b2) and (b4)), where the region is enclosed with red rectangle. (a) The first pair of underwater images; (b) The second pair of underwater images

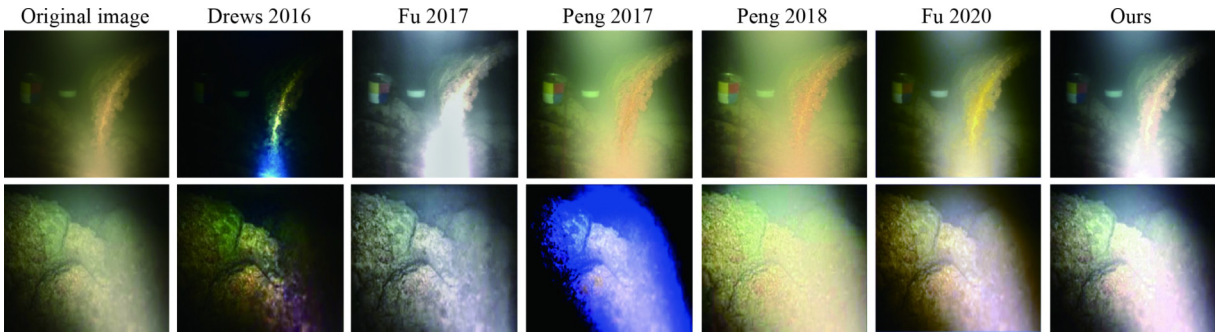

Fig. 15 Failure cases for underwater image dehazing. From left to right are original images, the results of Drews 2016 [5], Fu 2017 [33], Peng 2017 [26], Peng 2018 [29], Fu 2020 [2], and our proposed method

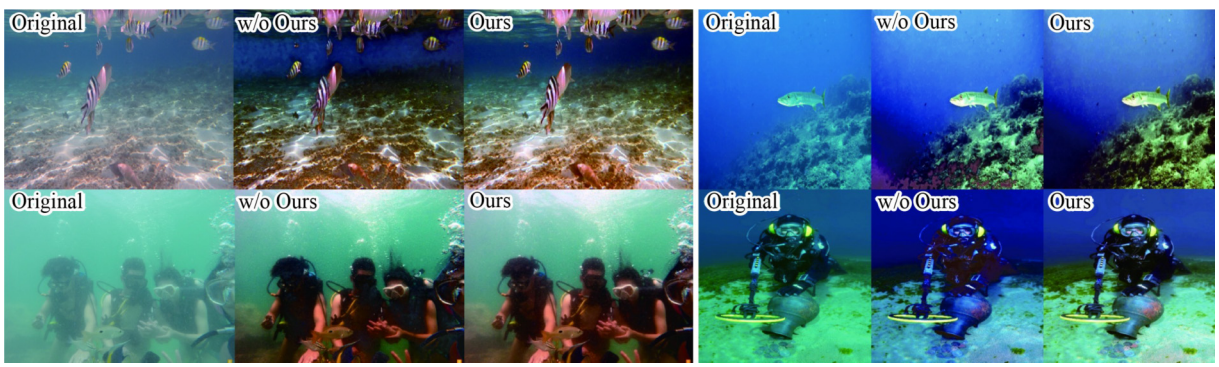

Fig. 16 Ablation study of the effect of correct background light estimation in our proposed method

Table 4 Quantitative evaluation of ablation study on UIEB dataset in terms of PSNR, SSIM, UCIQE and Entropy metrics respectively. The best results are highlighted in red

Method	Full-reference Metrics		Non-reference Metrics	
	PSNR↑	SSIM↑	UCIQE↑	Entropy↑
w/o Ours	18.9534	0.8109	0.6394	7.4720
Ours	19.9451	0.8466	0.6454	7.6090

obtain relatively genuine color and natural appearance. Based on the accurate background light estimation and enhanced transmission map, our method can further work well for a great variety of underwater images in terms of both subjective and objective evaluations.

Although this work provides an effective step-by-step model for underwater image enhancement, the computational time can be further reduced for practical applications. Moreover, underwater images with active light source as tough issue should also be addressed by integrating non-uniform illumination processing in our future work.

Acknowledgements This work was supported by Higher Education Scientific Research Project of Ningxia (NGY2017009).

References

1. Li C, Guo C, Ren W, Cong R, Hou J, Kwong S, Tao D. An underwater image enhancement benchmark dataset and beyond. IEEE Transactions on Image Processing, 2020, 29: 4376–4389
2. Fu X, Cao X. Underwater image enhancement with global-local networks and compressed-histogram equalization. Signal Processing: Image Communication, 2020, 86: 115892
3. Drews P Jr, do Nascimento E, Moraes F, Botelho S, Campos M. Transmission estimation in underwater single images. In: Proceedings of the IEEE International Conference on Computer Vision Workshops. 2013, 825−830
4. Galdran A, Pardo D, Picón A, Alvarez-Gila A. Automatic red-channel underwater image restoration. Journal of Visual Communication and Image Representation, 2015, 26: 132–145
5. Drews P L J, Nascimento E R, Botelho S S C, Campos M F M. Underwater depth estimation and image restoration based on single images. IEEE Computer Graphics and Applications, 2016, 36(2): 24–35
6. Peng Y T, Cosman P C. Single image restoration using scene ambient light differential. In: Proceedings of the 2016 IEEE International Conference on Image Processing (ICIP). 2016, 1953−1957
7. Lu H, Li Y, Xu X, Li J, Liu Z, Li X, Yang J, Serikawa S. Underwater image enhancement method using weighted guided trigonometric filtering and artificial light correction. Journal of Visual Communication and Image Representation, 2016, 38: 504–516
8. Li C, Guo J, Guo C, Cong R, Gong J. A hybrid method for underwater image correction. Pattern Recognition Letters, 2017, 94: 62–67
9. Zhuang P, Li C, Wu J. Bayesian retinex underwater image enhancement. Engineering Applications of Artificial Intelligence, 2021, 101: 104171
10. Zhang W, Dong L, Zhang T, Xu W. Enhancing underwater image via color correction and Bi-interval contrast enhancement. Signal Processing: Image Communication, 2021, 90: 116030
11. Chen L, Jiang Z, Tong L, Liu Z, Zhao A, Zhang Q, Dong J, Zhou H. Perceptual underwater image enhancement with deep learning and physical priors. IEEE Transactions on Circuits and Systems for Video Technology, 2021, 31(8): 3078–3092
12. Li C, Anwar S, Hou J, Cong R, Guo C, Ren W. Underwater image enhancement via medium transmission-guided multi-color space embedding. IEEE Transactions on Image Processing, 2021, 30: 4985–5000
13. Wen H, Tian Y, Huang T, Gao W. Single underwater image enhancement with a new optical model. In: Proceedings of the 2013 IEEE International Symposium on Circuits and Systems (ISCAS). 2013, 753−756
14. Emberton S, Chittka L, Cavallaro A. Hierarchical rank-based veiling light estimation for underwater dehazing. In: Proceedings of the British Machine Vision Conference (BMVC). 2015, 125.1−125.12
15. Zhou Y, Wu Q, Yan K, Feng L, Xiang W. Underwater image restoration using color-line model. IEEE Transactions on Circuits and Systems for Video Technology, 2019, 29(3): 907–911
16. Iqbal K, Odetayo M, James A, Salam R A, Talib A Z H. Enhancing the low quality images using unsupervised colour correction method. In: Proceedings of the 2010 IEEE International Conference on Systems, Man and Cybernetics. 2010, 1703−1709
17. Ghani A S A, Isa N A M. Enhancement of low quality underwater image through integrated global and local contrast correction. Applied Soft Computing, 2015, 37: 332–344
18. Ghani A S A, Isa N A M. Underwater image quality enhancement through integrated color model with Rayleigh distribution. Applied Soft Computing, 2015, 27: 219–230
19. Wang Y, Zhang J, Cao Y, Wang Z. A deep CNN method for underwater image enhancement. In: Proceedings of the 2017 IEEE International Conference on Image Processing (ICIP). 2017, 1382−1386
20. Dudhane A, Hambarde P, Patil P, Murala S. Deep underwater image restoration and beyond. IEEE Signal Processing Letters, 2020, 27: 675–679
21. Islam J, Xia Y, Sattar J. Fast underwater image enhancement for improved visual perception. IEEE Robotics and Automation Letters, 2020, 5(2): 3227–3234
22. Carlevaris-Bianco N, Mohan A, Eustice R M. Initial results in underwater single image dehazing. In: Proceedings of the Oceans 2010 MTS/IEEE Seattle. 2010, 1−8
23. Chiang J Y, Chen Y C. Underwater image enhancement by wavelength compensation and dehazing. IEEE Transactions on Image Processing, 2012, 21(4): 1756–1769
24. Lu H M, Li Y J, Zhang L F, Serikawa S. Contrast enhancement for images in turbid water. Journal of the Optical Society of America A, 2015, 32(5): 886–893
25. Li C Y, Guo J C, Cong R M, Pang Y W, Wang B. Underwater image enhancement by dehazing with minimum information loss and histogram distribution prior. IEEE Transactions on Image Processing, 2016, 25(12): 5664–5677
26. Peng Y T, Cosman P C. Underwater image restoration based on image blurriness and light absorption. IEEE Transactions on Image Processing, 2017, 26(4): 1579–1594
27. Berman D, Treibitz T, Avidan S. Diving into haze-lines: color restoration of underwater images. In: Proceedings of the British Machine Vision Conference (BMVC). 2017, 1−12
28. Wang Y, Liu H, Chau L P. Single underwater image restoration using adaptive attenuation-curve prior. IEEE Transactions on Circuits and Systems I: Regular Papers, 2018, 65(3): 992–1002
29. Peng Y T, Cao K, Cosman P C. Generalization of the dark channel prior for single image restoration. IEEE Transactions on Image Processing, 2018, 27(6): 2856–2868
30. Ancuti C, Ancuti C O, Haber T, Bekaert P. Enhancing underwater images and videos by fusion. In: Proceedings of the 2012 IEEE Conference on Computer Vision and Pattern Recognition. 2012, 81−88
31. Fu X, Zhuang P, Huang Y, Liao Y, Zhang X P, Ding X. A Retinex-based enhancing approach for single underwater image. In: Proceedings of the 2014 IEEE International Conference on Image Processing (ICIP). 2014, 4572−4576
32. Zhang S, Wang T, Dong J, Yu H. Underwater image enhancement via extended multi-scale Retinex. Neurocomputing, 2017, 245: 1–9
33. Fu X, Fan Z, Ling M, Huang Y, Ding X. Two-step approach for single underwater image enhancement. In: Proceedings of the 2017 International Symposium on Intelligent Signal Processing and Communication Systems (ISPACS). 2017, 789−794
34. Ancuti C O, Ancuti C, De Vleeschouwer C, Bekaert P. Color balance and fusion for underwater image enhancement. IEEE Transactions on Image Processing, 2018, 27(1): 379–393
35. Ancuti C O, Ancuti C, De Vleeschouwer C, Sbert M. Color channel compensation (3C): a fundamental pre-processing step for image enhancement. IEEE Transactions on Image Processing, 2020, 29: 2653–2665
36. Li J, Skinner K A, Eustice R M, Johnson-Roberson M. WaterGAN: unsupervised generative network to enable real-time color correction of monocular underwater images. IEEE Robotics and Automation Letters, 2018, 3(1): 387–394
37. Zhu J Y, Park T, Isola P, Efros A A. Unpaired image-to-image translation using cycle-consistent adversarial networks. In: Proceedings of the IEEE International Conference on Computer Vision. 2017, 2242−2251
38. Li C, Guo J, Guo C. Emerging from water: underwater image color correction based on weakly supervised color transfer. IEEE Signal Processing Letters, 2018, 25(3): 323–327
39. Guo Y, Li H, Zhuang P. Underwater image enhancement using a multiscale dense generative adversarial network. IEEE Journal of Oceanic Engineering, 2020, 45(3): 862–870
40. Li C, Anwar S, Porikli F. Underwater scene prior inspired deep

underwater image and video enhancement. Pattern Recognition, 2020, 98: 107038
41. Berman D, Treibitz T, Avidan S. Non-local image dehazing. In: Proceedings of the IEEE Conference on Computer Vision and Pattern Recognition. 2016, 1674−1682
42. Wang B, Li C. A visual hierarchical framework based model for underwater image enhancement. Frontiers of Computer Science, 2019, 13(3): 665–667
43. Wang B, Wei B, Kang Z, Hu L, Li C. Fast color balance and multi-path fusion for sandstorm image enhancement. Signal, Image and Video Processing, 2021, 15(3): 637–644
44. Gao S B, Zhang M, Zhao Q, Zhang X S, Li Y J. Underwater image enhancement using adaptive retinal mechanisms. IEEE Transactions on Image Processing, 2019, 28(11): 5580–5595
45. Xu Y, Wen J, Fei L, Zhang Z. Review of video and image defogging algorithms and related studies on image restoration and enhancement. IEEE Access, 2016, 4: 165–188
46. Yang M, Sowmya A. An underwater color image quality evaluation metric. IEEE Transactions on Image Processing, 2015, 24(12): 6062–6071
47. Finlayson G D, Trezzi E. Shades of gray and colour constancy. In: Proceedings of the Twelfth Color Imaging Conference: Color Science and Engineering Systems, Technologies, and Applications. 2004, 37−41
48. Land E H. The Retinex theory of color vision. Scientific American, 1977, 237(6): 108–128
49. Buchsbaum G. A spatial processor model for object colour perception. Journal of the Franklin Institute, 1980, 310(1): 1–26
50. van de Weijer J, Gevers T, Gijsenij A. Edge-based color constancy. IEEE Transactions on Image Processing, 2007, 16(9): 2207–2214
51. Kareem H H, Daway E G, Daway H G. No reference quality of the hazy images depending on transmission component estimation. IIUM Engineering Journal, 2019, 20(2): 70–77
52. Harris C, Stephens M. A combined corner and edge detector. In: Proceedings of the 4th Alvey Vision Conference. 1988, 147−151
53. Lowe D G. Distinctive image features from scale-invariant keypoints. International Journal of Computer Vision, 2004, 60(2): 91–110
54. Cheng M M, Mitra N J, Huang X L, Torr P H S, Hu S M. Global contrast based salient region detection. IEEE Transactions on Pattern Analysis and Machine Intelligence, 2015, 37(3): 569–582

Bo Wang received his PhD degree from the School of Electrical and Information Engineering, Tianjin University, China in 2016. He is currently a lecture in the School of Physics and Electronic-Electrical Engineering, Ningxia University, China. His research interests include image restoration and enhancement, image classification and medical image processing.

Zitong Kang received the BS degree from the School of Automation and Electronic Engineering, Qingdao University of Science and Technology, China in 2019. She is currently studying in the School of Physics, Electronic and Electrical Engineering, Ningxia University, China, majoring in Electronic and Communication Engineering. Her research interests include computer vision and data mining.

Pengwei Dong received the BS degree in Ningxia University, China in 2020. He is currently working toward the MS degree in School of Physics and Electronic-Electrical Engineering in Ningxia University, China. His research interests include remote sensing image enhancement and computer vision.

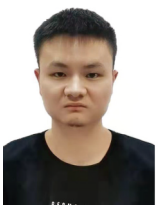

Fan Wang received the BS degree in University of South China, China in 2020. He is currently working toward the MS degree in School of Physics and Electronic-Electrical Engineering in Ningxia University, China. His research interests include medical image segmentation and computer vision.

Peng Ma received the BS degree in Ningxia University, China in 2020. He is currently working toward the MS degree in School of Physics and Electronic Electrical Engineering in Ningxia University, China. His research interests include computer vision and machine learning.

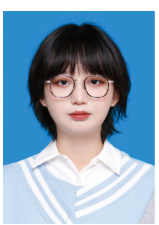

Jiajing Bai received the BS degree in Ningxia University, China in 2020. She is currently working toward the MS degree in School of Physics and Electronic-Electrical Engineering in Ningxia University, China. Her research interests include image processing and computer vision.

Pengwei Liang received the BS degree in Tianjin University of Technology, China in 2019. He is currently working toward the MS degree in School of Physics and Electronic-Electrical Engineering in Ningxia University, China. His research interests include image processing and computer vision.

Chongyi Li received the PhD degree from the School of Electrical and Information Engineering, Tianjin University, China in June 2018. From 2016 to 2017, he was a joint-training PhD Student with Australian National University, Australia. He was a postdoctoral fellow with the Department of Computer Science, City University of Hong Kong, China. He is currently a research fellow with the School of Computer Science and Engineering, Nanyang Technological University (NTU), Singapore. His current research focuses on image processing, computer vision, and deep learning, particularly in the domains of image restoration and enhancement.